Thayanithi Velusamy, Rajesh Krishnan, Kannapiran Nagarajan and Arularasan Palanisamy\*

# Structure, optical, thermal, dielectric, hardness behaviors of L-histidine barium nitrate (LHBN): a metal-organic crystal for optoelectronic applications

https://doi.org/10.1515/zkri-2025-0010 Received February 1, 2025; accepted November 3, 2025; published online November 26, 2025

Abstract: In the search for advanced materials for photonics and optoelectronic device fabrications, L-histidine – based metal - organic crystals have shown a remarkable contribution due to their nonlinear optical properties. However, the comprehensive investigations incorporating structural, thermal, mechanical and dielectric properties into a single framework remain scarce. In the current work, we report the growth of a novel semi-organic nonlinear optical crystal, L-histidine barium nitrate (LHBN), using the slow cooling technique. The synthesis involves mixing histidine and barium nitrate in a 1:1 M ratio. Single crystals of approximately 10 mm in size were obtained within 45 days. The crystallization process of LHBN was confirmed through single crystal X-ray diffraction analysis, revealing a monoclinic system with non-centrosymmetric space group C2. FTIR spectroscopy was used to find functional group vibrations and the transmission spectrum was recorded in the solution state to show the lower cut-off frequency. The materials exhibited excellent optical transparency with a lower cut-off wavelength at 226 nm. Thermal stability of the grown crystal up to 240 °C was observed using TGA/DTA analysis. The mechanical and dielectric properties of the grown LHBN crystals were evaluated along the (0 1 0) crystallographic plane. Dielectric analysis proved the frequency dependent permittivity with low dielectric loss at high frequencies, which makes the materials for NLO applications. Additionally, the optical nonlinearity of the crystal was confirmed

using the Kurtz powder technique, which demonstrated its high second harmonic generation efficiency with 2.2 times that of KDP.

**Keywords:** L-Histidine; X-rays diffraction; FTIR; TG analyses; SHG

#### 1 Introduction

The design of highly effective optical crystals with strong nonlinearity has been extensively studied due to its applications in electro-optical modulation, terahertz (THz) generation, ultrafast switches, laser amplifiers, optical parametric oscillation, frequency conversion, optical communication, and other advanced technological devices. 1-3 The incorporation of both organic and inorganic materials has garnered significant attention, as it enhances the nonlinear optical (NLO) properties of the resulting crystals. Semi-organic crystals, particularly amino acid metal complexes, exhibit high NLO coefficients and strong optical transmission in the visible region, outperforming inorganic crystals. Furthermore, semi-organic materials have higher laser damage thresholds, greater thermal stability, and superior mechanical properties than organic crystals. These enhanced properties make semi-organic crystals ideal candidates for optoelectronic and laser processing applications. 4-6

Various crystalline derivatives of amino acids have been investigated to identify new NLO materials. Amino acids, as examples of molecular chirality, constitute a proton donor carboxyl group (COOH) and a proton acceptor amino group (NH<sub>2</sub>). In the search for novel NLO materials, compounds containing both electron acceptors and donor substituents have been synthesised and studied. Several nonlinear optical crystals with second-harmonic generation (SHG) efficiencies similar to potassium dihydrogen phosphate (KDP) have been discovered. Butyl-histidine crystals, in particular, exhibit excellent nonlinearity and quick optical response while maintaining acceptable physico-chemical stability. L-histidine derivatives exhibit high NLO properties due to

Higher Education, Coimbatore, Tamilnadu, 641021, India

<sup>\*</sup>Corresponding author: Arularasan Palanisamy, Postgraduate
Department of Physics, Dwaraka Doss Goverdhan Doss Vaishnav College,
Chennai, Tamilnadu, 600107, India, E-mail: aruldgvc@gmail.com
Thayanithi Velusamy, Department of Physics, Nandha Engineering
College (Autonomous), Erode, Tamilnadu, 638052, India
Rajesh Krishnan, Department of Physics, Dayananda Sagar College of
Engineering, Bengaluru, 560111, India
Kannapiran Nagarajan, Department of Chemistry, Karpagam Academy of

the presence of an imidazole group, in addition to the aminocarboxylate assembly. 11–14

Several L-histidine-based crystals, such as L-histidinium acetate dihydrate. L-histidine methylester dihydrochloride. L-histidine maleate-(1.5)-hydrate, L-histidine L-aspartate monohydrate, L-histidine hydrofluoride dihydrate and L-histidine glutrate monohydrate, have been synthesised and their optical properties have been reported recently. These L-histidine derivatives have exceptional optical performance and will be considered as a potential candidate for the fabrication of photonic device construction. 15-20

In spite of various L-histidine crystals having been synthesised and reported for their high nonlinear optical nature, most of these studies focus primarily on either structural or optical properties in isolation. But our work on L-histidine barium nitrate (LHBN) provides a detailed investigation encompassing structural properties, optical transparency, thermal behaviour, dielectric nature, micro hardness and NLO efficiency. Notably, this is the first report on the successful integration of barium nitrate with L-histidine to form a non-centrosymmetric metal organic crystal with improved NLO efficiency, proving it a huge contribution to the class of semi-organic crystals for optoelectronic applications. The title compound, L-histidine barium nitrate (LHBN), is a semi-organic crystal that contains molecular entities with delocalised electrons, as well as additional electron acceptor and donor groups. The present study aims to investigate the mechanical, structural, electrical, and thermal properties of LHBN crystals as well as vibrational assignments derived from infrared and Raman spectroscopy techniques.

### 2 Synthesis of L-histidine barium nitrate (LHBN) single crystal

L-histidine barium nitrate (LHBN) single crystal was synthesised by reacting L-histidine (Sigma Aldrich, ≥99 %) with barium nitrate (Merck, ≥99 %) at a molar ratio of 2:1. The reactants were dissolved in deionized water, and the solution was agitated using a hot plate magnetic stirrer with a temperature controller to ensure uniform mixing. The temperature was kept between 45 °C and 55 °C during this process. The resultant solution was allowed to evaporate at room temperature, causing the formation of LHBN crystals. The synthesized salts were then recrystallized to obtain pure samples. A schematic representation of the materialization and reaction process for L-histidine barium nitrate single crystals is provided below.

To prepare a saturated solution, 100 mL of purified LHBN was dissolved at 35 °C. The solution was filtered using a 250 mL glass beaker and microfilters to remove any impurities. After filtration, the beaker was sealed and placed in a cryostat bath. The temperature of the solution was gradually lowered at a rate of 0.1 °C/day. After a typical growth period of 45 days, single crystals of LHBN were successfully grown. A representative image of the obtained LHBN crystals is shown in Figure 1.

#### 3 Results and discussion

#### 3.1 Crystallographic details of LHBN

The X-ray intensity data for L-histidine barium nitrate (LHBN) single crystals were collected using a Bruker APEX II single-crystal X-ray diffractometer equipped with MoKα radiation ( $\lambda$  = 0.71073 Å). The  $\omega$ /2 $\theta$  scan method was employed for data acquisition. A crystal with dimensions of  $0.18 \times 0.14 \times 0.12$  mm<sup>3</sup> was used for the analysis. The unit cell parameters for the as-grown LHBN crystal were determined to be: a = 24.9063(8) Å, b = 4.7226(10) Å, c = 8.3180(3) Å,  $\alpha = 90^{\circ}$ ,  $\beta$  = 105.43(10)°,  $\gamma$  = 90°, and the unit cell volume was calculated to be 943.11(5) Å<sup>3.21</sup> The crystallographic data for the as-grown LHBN crystal are summarized in Table 1. observed limiting indices were be  $-39 \le h \le 40$ ,  $-6 \le k \le 7$ ,  $-13 \le l \le 11$  and a total of 2117 unique reflections were recorded out of 6598 measured reflections.

The integrated intensities were corrected for Lorentz. polarization, and decay factors. Absorption corrections were applied using the psi-scan method. For structure refinement all observed reflections were used to refine the lattice parameters. The maximum and minimum transmission factors were determined to be 0.7799 and 0.6950, respectively. The crystal structure was solved by direct methods using the program SIR92 within the WINGX package and refinement was carried out by SHELXL97.<sup>22,23</sup> The ORTEP plot of LHBN, showing the ellipsoid representation at the 35% probability level, is depicted in Figure 2.

#### 3.2 Crystal structure of LHBN

Histidine derivatives play a crucial role in various biochemical and biomolecular interactions. The geometric parameters of the L-histidine moiety in L-histidine barium

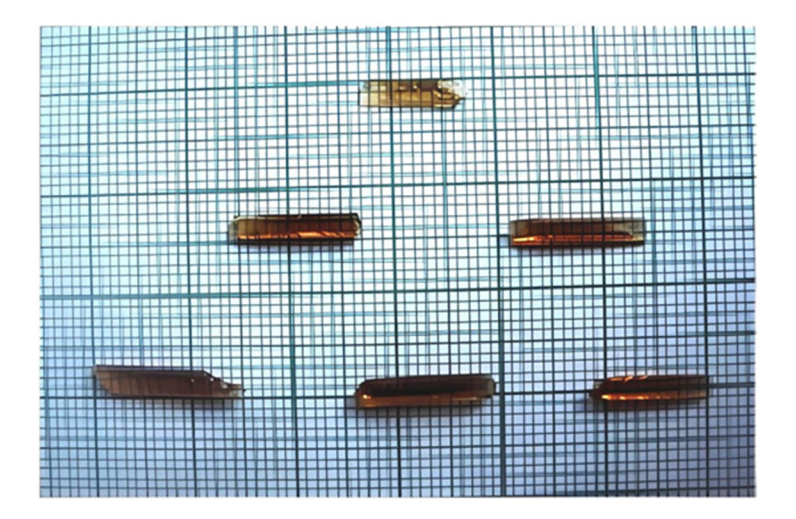


Figure 1: Photography of LHBN.

Table 1: Crystal data and structure refinement for LHBN.

Parameter	LHBAN (This Work)	LHTFB [Ref. 24]
Crystal system	Monoclinic	Monoclinic
Space group	C2	P2 <sub>1</sub>
a (Å)	24.9063(8)	9.482(2)
b (Å)	4.7226(10)	6.894(1)
c (Å)	8.3180(3)	13.021(3)
β (°)	105.43(10)	103.47(2)
Volume (Å <sup>3</sup> )	943.11(5)	821.1(3)
Coordination	Ba <sup>2+</sup> coordinated with 10 O	No metal ion; proton-
environment	atoms (6 from $L$ -histidine, 4 from $NO_3^-$ )	ated L-histidine interacts with BF <sub>4</sub> <sup>-</sup>
Hydrogen	N-H···O and N-H···N	N-H···O and N-H···F
bonding	forming 1D chains along	bonding with BF <sub>4</sub> units
interactions	[010]	
Structural distinction	Metal-coordinated frame- work with polymeric chains	Discrete ion pairs, sta- bilized by hydrogen bonding

Figure 2: Thermal ellipsoidal projection (ORTEP) of LHBN.

nitrate (LHBN) are similar to those observed in previously reported structures.<sup>24</sup> The crystallographic analysis reveals a twofold symmetry axis, with the barium atom located at the center and coordinated by ten oxygen atoms. Six of these oxygen atoms are orginated from the carboxylate groups of L-histidine, while the remaining four contributed by two nitrate groups. The Ba-O bond distances range from 2.767(5)

to 2.966(2) Å, which is within the expected range for such interactions. The LHBN molecules are linked through oxygen atoms, forming a one-dimensional chain along the [010] direction. These chains are further stabilized by N–H $\cdots$ N and N-H...O hydrogen bonding interactions, which interconnect the structures.

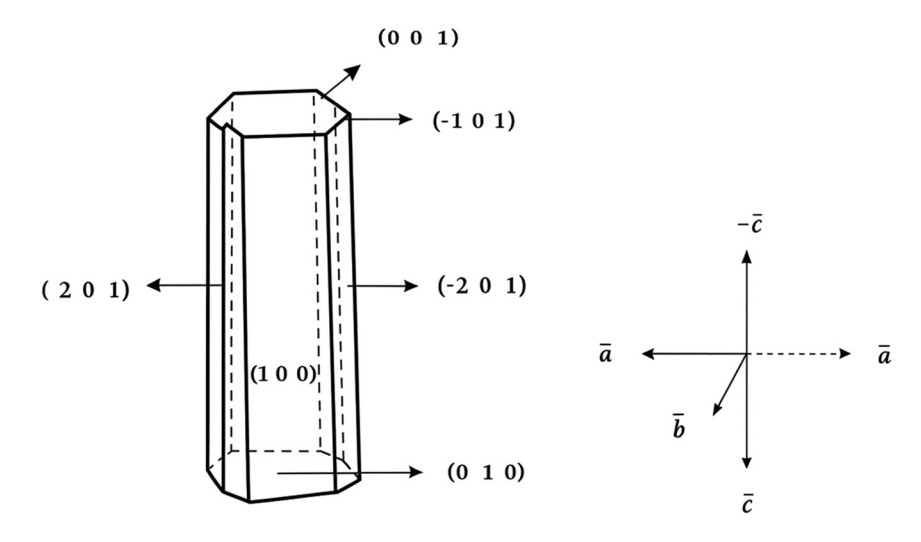


Figure 3: Morphology of LHBN.

#### 3.3 Morphological studies of LHBN

The L-histidine barium nitrate (LHBN) crystal exhibits six visible faces. Four of these faces, namely (0 1 0), (0 0 1), (1 0 0), and (2 0 1), are well-defined, as shown in Figure 3. The (1 0 0) face is identified as the largest flat face. The normal to this prominent flat face is oriented along the – c direction. The three crystallographic directions, a, b, and c, are also indicated in Figure 3. The c and –c directions are found to be nearly parallel, make an angle of  $\beta$  = 92.30°. The growth rate along the c-axis is observed to be greater than that along the other axes, while the crystal grows more slowly along the b-axis.

#### 3.4 Spectral studies of LHBN

The infrared (IR) and Raman spectra of L-histidine barium nitrate (LHBN), presented in Figures 4 and 5, respectively, and primarily attributed to the vibrational modes of the L-histidine cation and its associated groups. The observed bands and their corresponding assignments are summarized in Table 2. All spectral data were compared with standard reference data reported in the literature.

The  $(N-H\cdots O)$  hydrogen bonding network, formed between the amino hydrogen atoms of the cation and the oxygen atoms of adjacent anions, plays a crucial role in achieving non-centrosymmetry within the crystal structure.

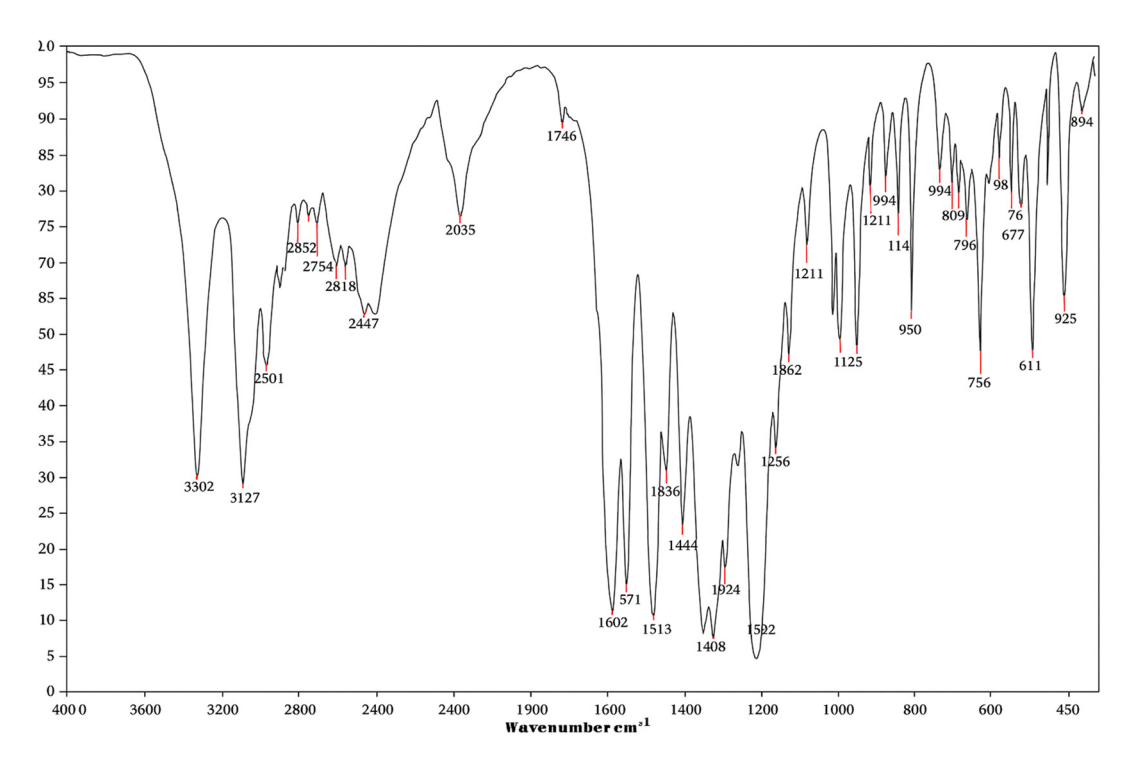


Figure 4: FTIR spectrum of LHBN single crystal.

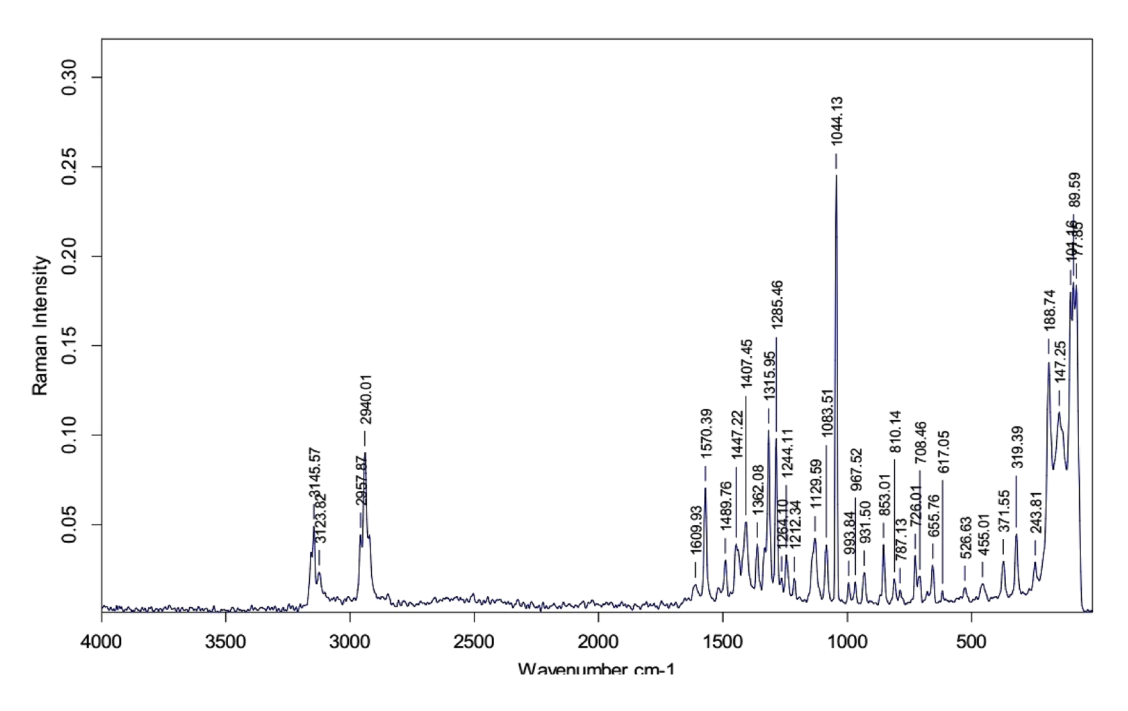


Figure 5: FT Raman spectrum of LHBN single crystal.

Table 2: Comparison of IR and Raman frequencies of LHBN.

IR	Raman	Assignment
frequencies cm <sup>-1</sup>	frequencies cm <sup>-1</sup>	Assignment
3,362	_	O–H stretching
3,127	3,145	C-H symmetric stretching
3,003	3,123	C-H asymmetric stretching
2,852	_	N–H stretching
-	2,957	CH symmetric stretching
-	2,940	CH <sub>2</sub> symmetric stretching
2,447	-	Combination tones
2,035	_	Combination tones
1,746	_	C=O symmetric stretching
1,602	1,609	COO <sup>-</sup> asymmetric stretching
-	1,570	Combination tones
1,488	1,489	N–H bending
1,449	1,447	CH <sub>3</sub> asymmetric bending
1,384	1,362	CH <sub>3</sub> symmetric bending
1,286	1,285	C-O stretching
1,141	1,129	C–N wagging
1,079	1,083	C-N symmetric stretching
-	967	NH <sub>2</sub> bending
854	853	N–H wagging
-	787	CNH stretching
677	_	C-H bending
630	658	COO bending
487	455	NH <sub>2</sub> rocking

In the IR spectrum, the stretching vibration of the O–H bond is observed at  $3,362~\rm cm^{-1}$  but is absent in the Raman spectrum. The band at  $3,127~\rm cm^{-1}$  in the IR spectrum is assigned to the stretching vibrations of the C–H bonds in the imidazole

ring,<sup>13</sup> with a corresponding Raman line detected at 3,145 cm<sup>-1</sup>. In the spectra of LHBN, these bands appear slightly shifted: 3,127 and 3,003 cm<sup>-1</sup> in the IR, spectrum and 3,145 and 3,123 cm<sup>-1</sup> in the Raman spectrum. The presence of such sharp and well-defined bands in this region is characteristic of histidine salts.<sup>20</sup>

The stretching vibrations of aliphatic CH and CH2 groups are observed at 2,957 cm<sup>-1</sup> and 2,940 cm<sup>-1</sup>, respectively, in the Raman spectrum. In contrast, the corresponding stretching vibrations of the C–H bonds in CH and CH2 groups are not detected in the IR spectrum. A band at 2,852 cm<sup>-1</sup> in the IR spectrum is likely attributed to the stretching of N–H bonds in the imidazole ring, with this vibration absent in the Raman spectrum. <sup>12,13</sup> The band observed at 1,746 cm<sup>-1</sup> in the IR spectrum is associated with the C=O stretching vibrations of the carboxyl group. This characteristic band is absent in the Raman spectrum. The asymmetric stretching vibrations of the carboxylate group are observed at 1,602 cm<sup>-1</sup> and 1,609 cm<sup>-1</sup> in the IR and Raman spectra, respectively.

The bending vibration of the amino group is observed at 1,488 cm<sup>-1</sup> and 1,489 cm<sup>-1</sup> in IR and Raman spectra, respectively. The bands at 1,079 cm<sup>-1</sup> and 1,083 cm<sup>-1</sup> in both spectra correspond to the symmetric stretching vibrations of the nitrate ion. A band at 967 cm<sup>-1</sup> is detected in the Raman spectrum correspondence to the bending of the NH2 group and is absent in the IR spectrum. A band at 854 cm<sup>-1</sup> in IR and 853 cm<sup>-1</sup>in Raman spectra are attributed to the wagging of the NH group. Additionally a broad band associated with the CNH group is observed at 787 cm<sup>-1</sup> in the IR spectrum.

A pronounced band at 677 cm<sup>-1</sup> in the FTIR spectrum corresponds to the bending vibration of the CH group, while its counterpart does not appear in the Raman spectrum. The bending vibration of the carboxylate group is indicated by peaks at 655 cm<sup>-1</sup> in the FTIR and 656 cm<sup>-1</sup> in the Raman spectrum. The rocking vibration of the amino group is observed at 487 cm<sup>-1</sup> in the FTIR spectrum and 455 cm<sup>-1</sup> in the Raman spectrum. The band positions in both the FTIR and Raman spectra exhibit good agreement, and the observed results are consistent with those reported for other L-histidine complexes.<sup>25,26</sup>

#### 3.5 UV-visible absorption spectrum of LHBN

The absorption spectrum of L-histidine barium nitrate (LHBN) single crystal was recorded in the wavelength range of 200–800 nm using a Varian Cary 5E UV–visible Spectrometer, and the results are displayed in Figure 6. The lower

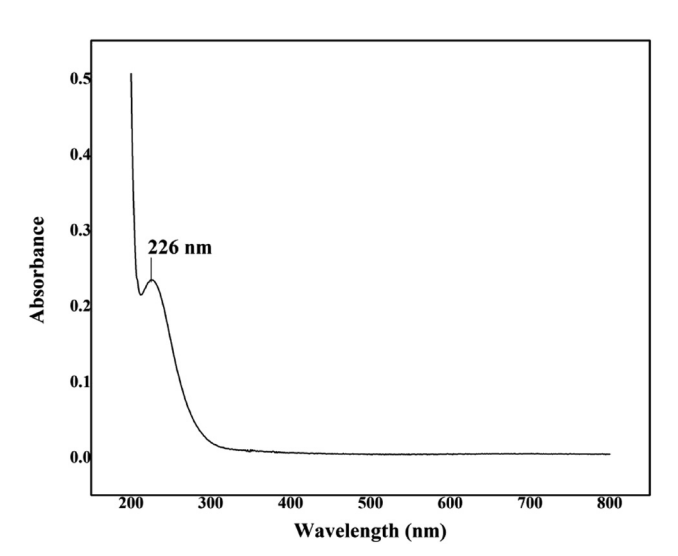
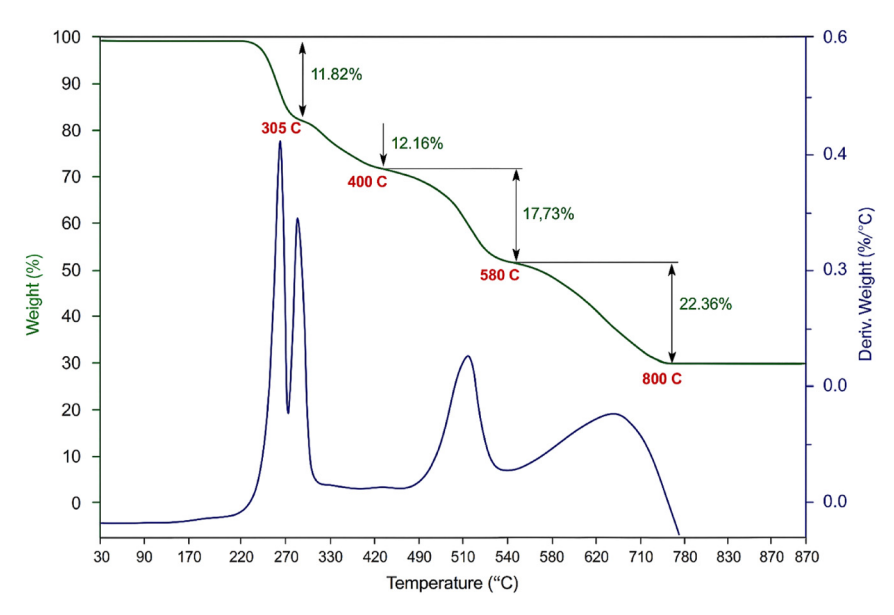


Figure 6: UV-visible spectrum of LHBN.



cutoff wavelength for LHBN was found to be 226 nm. The crystal exhibits optical transparency in the wavelength range of 250–800 nm, with absorbance values remaining below one unit between 300 and 800 nm. This optical behavior is particularly beneficial for potential applications in optoelectronic device fabrication and higher-order harmonic generation. <sup>18</sup>

#### 3.6 Thermal analysis of LHBN

Thermal analysis of the grown L-histidine barium nitrate (LHBN) crystals was performed to assess their thermal stability and melting point. Thermogravimetric analysis (TGA) and differential thermal analysis (DTA) were carried out using a NETZSCH STA 409C thermal analyzer in the temperature range of 26–800 °C at a heating rate of 10 °C/min, as shown in Figure 7. An alumina crucible was employed for heating the sample, and the analysis was carried out in a nitrogen atmosphere.

From the TGA curve, it is evident that LHBN is thermally stable upto 240 °C, indicating greater thermal stability compared to other L-histidine compounds. <sup>27–29</sup> The thermal stability is attributed to the strong bonding between the NH<sub>3</sub>+ group and the barium metal ion, which stabilizes the crystal structure The endothermic peak observed at 305 °C in the DTA curve corresponds to the melting point of LHBN. Thermal degradation of LHBN noticed between 240 and 360 °C in different stages. In this first stage a weight loss of 11.82 % correspondence by the release of NH3. During the second stage (330–450 °C), 12.16 % loss is due to the decomposition of the volatile substance like CO and CO2. During the last stage at 360–580 °C, almost 18 % of weight is eliminated. In this stage most of organic materials are oxidized and NO2 gas. An additional

Figure 7: TG-DTA curve of LHBN.

endothermic peak at 580 °C indicates complete decomposition of the LHBN crystal. At 800 °C (22.36 %), leaving behind inorganic barium residues of BaO.

#### 3.7 Dielectric measurements of LHBN

The capacitance and dissipation factor were restrained for the (0 1 0) plane of the LHBN crystal in the frequency series of 100 Hz to 5 MHz at 313, 323, 373, and 423 K. Dielectric constant ( $\varepsilon_r$ ), dielectric loss (tan  $\delta$ ) were considered by means of the equation

$$\varepsilon_r = \mathrm{Cd}/\varepsilon_0 \mathrm{A}$$
 and  $\tan \delta = \varepsilon_r \mathrm{D}$ .

The values of  $\varepsilon_r$  and  $\tan\delta$  are shown in Figures 8 and 9 as a function of frequency at different temperatures. The dielectric polarization in total of the material is from the contribution of dipolar, electronic, space and ionic, charge polarization at inferior frequencies and the value of  $\varepsilon_r$  rises primarily due to the low frequency range between 100 Hz and 5 MHz which is produced due to the orientation of the dipoles.

The lower rate of dielectric value at high frequency is a suitable constraint for enhancing SHG competence. The decreasing dielectric constant  $\varepsilon_r$  with increasing frequency is mostly attributed to the space charge polarizations of the grown LHBN crystal. The grown crystal with high optical quality encompasses fewer defects due to detected lower values of dielectric loss at higher frequencies moreover  $\varepsilon_r$  and  $\tan\delta$  increase with rise in temperature. This is due to the enhanced dipolar orientation and space charge polarization at higher temperatures. At higher frequencies, the dielectric

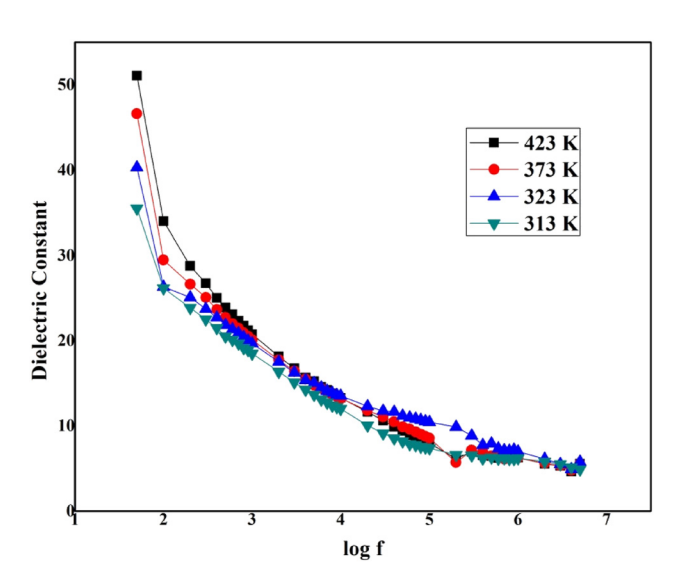


Figure 8: Log f versus dielectric constant of LHBN.

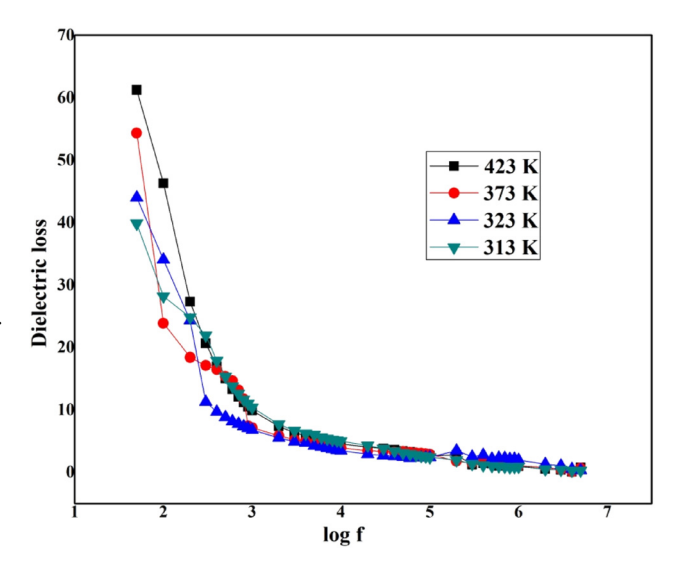


Figure 9: Log f versus dielectric loss of LHBN.

constant becomes relatively stable, as dipolar contributions lag behind the oscillating frequency. The low dielectric loss at high frequency shows that the crystal shows low energy dissipation, which makes the crystal suitable for nonlinear optical applications.  $^{31-33}$ 

The AC conductivity ( $\sigma_{ac}$ ) studies have been measured for the LHBN crystal using  $\sigma_{ac} = \epsilon_o \epsilon_r \omega \tan \delta$  where  $\omega$  is the angular frequency ( $\omega = 2\pi \nu$ ) of the applied field,  $\epsilon_r$  is the relative dielectric constant  $\epsilon_o$  is the vacuum dielectric constant (8.85 × 10<sup>-12</sup> farad/m). Figure 10 shows the deviance of ac conductivity with various temperatures and frequencies. It is perceived that the value of ac conductivity rises with a rise in frequency. AC conductivity of grown crystal increases

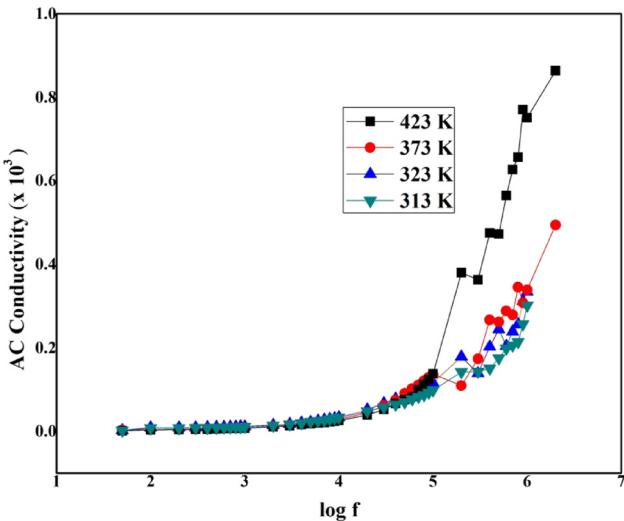


Figure 10: Log f versus AC conductivity of LHBN.

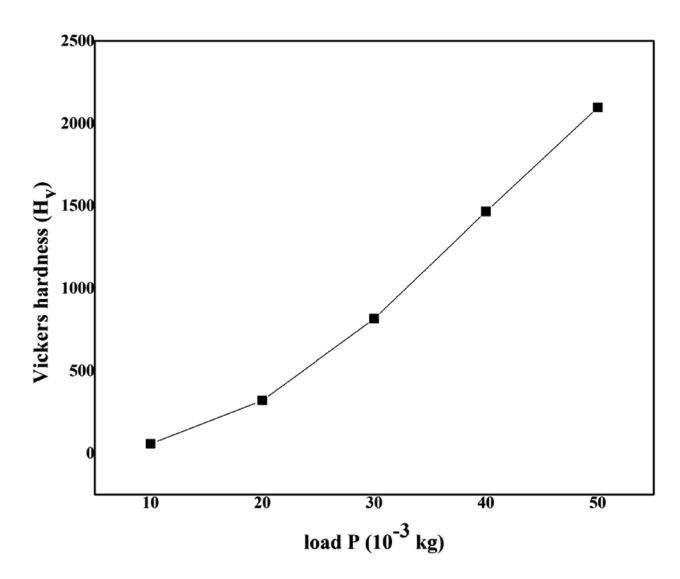


Figure 11: Microhardness of LHBN

with frequency, exhibiting the strength of hydrogen bonds in molecules and making it more suitable for optoelectronic applications. <sup>33,34</sup>

#### 3.8 Microhardness measurements of LHBN

The grown LHBN crystals were tested using Vicker's micro hardness tester along the (0 1 0) crystallographic plane. A constant indentation time of 15 s was deployed, and the applied load was varied from 5 to 50 g. The indentations impression along the diagonals of the sample was measured using Leitz Metallax II microscope. The  $H_{\nu}$  (Vickers micro hardness) of the crystal was calculated using the following relation

$$H_{\rm v} = 1.8544 \frac{P}{d^2} {\rm MPa}$$

where, d is the mean diagonal length of the indenter impression, P is the applied load, various loads of 10, 20, 30, 40, and 50 g were applied. Micro cracks were observed around the indentation site at the loads above 50 g and therefore, readings were not collected at higher loads above 50 g. A graph is drawn amongst  $H_{\nu}$  and applied load P (Figure 11). It is witnessed from the graph that the hardness value initially surges with the surge of the applied load by obeying the indentation size effect (ISE).  $^{35}$ 

## 3.9 Second harmonic generation (SHG) studies of LHBN

The second-harmonic generation (SHG) of L-histidine barium nitrate (LHBN) was investigated using the Kurtz and Perry

powder method, using Nd:YAG laser, operating at a wavelength of 1,064 nm. The as-grown LHBN crystal was finely ground into powder and loaded into a microcapillary with a uniform bore. A high-intensity laser beam was directed onto the sample and the SHG was confirmed by the emission of green light at 532 nm. The SHG efficiency of LHBN was compared to that of potassium dihydrogen phosphate (KDP). The SHG efficiency of LHBN was found to be 2.2 times that of KDP, indicating that the LHBN crystal exhibits a higher SHG efficiency compared to other L-histidine derivative crystals. <sup>36</sup>

#### 4 Conclusions

L-histidine barium nitrate (LHBN) single crystals were successfully grown using the slow evaporation method, yielding crystals with dimensions of  $9 \times 2 \times 2 \text{ mm}^3$ . Additionally, single crystals were synthesized via a slow cooling procedure. The novelty of this work lies in incorporating barium nitrate into the L-histidine, resulting in a 10-fold oxygen coordination around Ba<sup>2+</sup> ions and forming a unique 1-D chain structure stabilized by N-H...O and N-H...N hydrogen bonding. This structural arrangement enhances the material's optical and dielectric behavior. The LHBN crystal adopts a non-centrosymmetric monoclinic crystal system with a space group of C2. Morphological analysis shows that the prominent plane is along the (010) direction and is more optically translucent compared to the other planes. The presence of various functional groups and the hydrated nature of LHBN were confirmed through FT-Raman and FTIR analyses. The electronic transition band confirms good transparency of the crystal in the visible and near-infrared regions, with a lower cutoff wavelength at 226 nm. Thermogravimetric (TG) and differential thermal analysis (DTA) results show that LHBN remains thermally stable up to 240 °C. Dielectric measurements revealed that the low value of the dielectric constant at high frequencies contributes to the enhanced second-harmonic generation (SHG) efficiency of the material. The mechanical behavior of the crystal was evaluated through indentation size effect, providing insight into its hardness properties of the LHBN crystal. The powder SHG Measurements show that LHBN exhibits 2.2 times higher SHG efficiency thanthat of potassium dihydrogen phosphate (KDP) crystals. The higher efficiency can be attributed to the interaction between the electron-donating histidine and the electron-withdrawing nitrate groups within the polar, non-centrosymmetric lattice. Overall, the results prove that LHBAN as a new-generation metal-organic crystal with potential applications in optical switching,

themally stable optoelectronic devices and frequency doubling applications.

**Research ethics:** Not applicable. **Informed consent:** Not applicable.

Author contributions: All authors have accepted responsibility for the entire content of this manuscript and approved its submission.

Use of Large Language Models, AI and Machine Learning

Tools: None declared.

**Conflict of interest:** The authors state no conflict of interest.

Research funding: None declared. Data availability: Not applicable.

#### References

- 1. Cong, L.; Srivastava, Y. K.; Zhang, H.; Zhang, X.; Han, J.; Singh, R. All-Optical Active THz Metasurfaces for Ultrafast Polarization Switching and Dynamic Beam Splitting. Light: Sci. Appl. 2018, 7, 28.
- 2. Tan, Y.; Zhao, H.; Zhang, R.; Zhang, C.; Zhao, Y.; Zhang, L. Ultrafast Optical Pulse Polarization Modulation Based on the terahertz-induced Kerr Effect in low-density Polyethylene. Optical Express 2020, 28, 35330.
- 3. Arularasan, P.; Sindhusha, S.; Rajesh, K.; Gunasekaran, B.; Thayanithi, V. Experimental and Theoretical Investigation of Novel Organic L-Glutaminium Benzenesulfonate Single Crystal - DFT and Experimental Approach. Spectrochim. Acta Part A: Mol. Biomol. Spectrosc. **2023**, 286, 121985.
- 4. Liu, G.; Liu, J.; Zheng, X.; Liu, Y.; Yuan, D.; Zhang, X.; Gao, Z.; Tao, X. Bulk Crystal Growth and Characterization of Semi-organic Nonlinear Optical Crystal Tri-Diethylammonium hexachlorobismuthate (TDCB). CrystEngComm 2015, 17, 2569.
- 5. Chandran, S.; James, G. J.; Magesh, M.; Prasanna, N. Synthesis, Crystal Growth, Structural, Spectral, Laser Threshold Energy and Dielectric Properties of Lithium L-Tartrate Monohydrate Crystal. J. Mol. Struct. **2020**, 1223, 128988.
- 6. Chandran, S.; Paulraj, R.; Ramasamy, P. Nucleation Kinetics, Crystal Growth and Optical Studies on Lithium Hydrogen Oxalate Monohydrate Single Crystal. J. Cryst. Growth 2017, 468, 68-72.
- 7. Morimoto, H.; Unoura, K.; Nabika, H. Effect of Amino Acid Addition on the Crystallization of Asparagine. Cryst. Growth Des. 2021, 21, 2205-2211.
- 8. Rosalba, R.; Massimiliano, G.; Chiara, M. A. G.; Maria, E. F.; Roberto, P.; Alessandro, D. Chiral Recognition of L- and D- Amino Acid by Porphyrin Supramolecular Aggregates. Molecules 2019, 24, 84.
- 9. Thayanithi, V.; Praveen Kumar, P. Investigation on Optical, Laser Damage Threshold and Non Linear Optical Behavior of Creatininium p-Toluenesulfonate Crystal for Electro-Optical Applications. J. Mater. Sci.: Mater. Electron. 2020, 31, 22098-22106.
- 10. Abila Jeba Queen, M.; Bright, K. C.; Mary Delphine, S.; AjiUdhaya, P. Enhanced Linear and Non-linear Optical Activity of Lead Onto I-Threonine Cadmium Acetate Crystal. J. Mater. Sci.: Mater. Electron. **2021**, 32, 13261-13268.
- 11. Xueni, L.; Yan, R.; Cheng, Q. Z.; Bo, W.; Sheng, Q. X. Single-Crystalline Fibers of Deuterated Potassium Dihydrogen Phosphate. Crystals 2020, 10, 511.
- 12. Ian, F. S. R.; Jailton, R. V.; João, G. O. N.; Stanislav, R. S.; José, W. M. C.; Mateus, R. L.; Adenilson, O. S. Synthesis, Characterization, and Thermal

- and Computational Investigations of the I-histidine Bis(Fluoride) Crystal. J. Mol. Model. 2022, 28, 222.
- 13. Peer Mohamed, M.; Sudha, S.; Jayaprakash, P.; Vinitha, G.; Nageshwari, M.; Sangeetha, P.; RathikaThayaKumari, C.; Lydia Caroline, M. Growth and Characterization of L-Histidinium Fumarate Fumaric Acid Monohydrate Single Crystal: A Promising Second and Third Order Nonlinear Optical Material. Chin. J. Phys. 2019, 60, 581-597.
- 14. Holeček, M. Physiol. Res. 2020, 69, 555-564.
- 15. Albert, H. M.; Durgadevi, G.; Kanimozhi, D.; Alosious Gonsago, C. Structural, Spectroscopic, Dielectric, and Impedance Features of I-Histidinium Acetate Dihydrate Crystals for Optoelectronic Uses. Appl. Phys. A 2024, 130, 543.
- 16. Albert, H. M.; Ghodke, P. D.; Kumar, N. M.; Patnaik, D. N.; Indrakanti, R.; Uma, B.; Mallesh, M. P.; Alosious Gonsago, C. Exploring the Spectroscopic, Optical, Dielectric, and Hardness Properties of L-Histidine Methylester Dihydrochloride (LHMEDH), a Nonlinear Optical Compound for Optoelectronic Uses. Appl. Phys. A 2024, 130, 941.
- 17. Albert, H. M.; Thota, K.; Dharmadhikari, N. P.; Kasabe, S. M.; Babu, S. H.; Priya, R.; Farooq, S.; Alosious Gonsago, C. Investigations of the Structural, Spectral, Dielectric, and Electrical Characteristics of I-Histidine Maleate-(1.5)-Hydrate Crystals for Frequency Conversion Processes. J. Mater. Sci.: Mater. Electron. 2024, 35, 106.
- 18. Nalini, H.; Charles Vincent, V.; Bakiyaraj, G.; Kirubavathi, K.; Selvaraju, K. Structural, Optical, Laser Damage, NLO and Theoretical Analysis of I-Histidine I-Aspartate Monohydrate Crystals. Phys. B: Condens. Matter 2020, 592, 412245.
- 19. Kathiravan, V.; Satheesh Kumar, G.; Pari, S.; Selvarajan, P. Influence of Dye Doping on the Structural, Spectral, Optical, Thermal, Electrical, Mechanical and Nonlinear Optical Properties of L-Histidine Hydrofluoride Dihydrate Crystals. J. Mol. Struct. 2021, 1223, 128958.
- 20. Albert, H. M.; Priya, R.; Pandian, P. M.; Ganganagunta, S.; Prasad, S. V. G. V. A.; Patnaik, D. N.; Kumar, N. M. Crystallization, Structural, Dielectric, Mechanical, and SHG Studies of I-Histidine Glutarate Monohydrate Crystal for Nonlinear Optical Device Applications. J. Mater. Sci.: Mater. Electron. 2023, 34, 1822.
- 21. Arularasan, P.: Chakkaravarthi, G.: Mohan, R. Catena-Poly[[bis(nitrato- $\kappa^2$  O,O')barium]-bis( $\mu$ -l-histidine- $\kappa^3$  O,O':O]. *ActaCryst.* **2013**, *69*, m597.
- 22. Sheldrick, G. M. ActaCryst. 2008, A64, 112-122.
- 23. Sheldrick, G. M. Shells-97, Program for Crystal Structure Solution; University of Göttingen: Göttingen, Germany, 1997.
- 24. Gokul Raj, S.; Ramesh Kumar, G.; Mohan, R.; Pandi, S.; Jayavel, R. Structural, Optical and Dielectric Studies on Solution-Grown Semi-Organic I-Histidine Tetrafluoroborate Single Crystal. Mater. Chem. Phys. 2005, 90, 144-147.
- 25. Jin, L.; Sakiyan, I.; Gonzales, N. S.; Lane, D.; Cherala, S. Synthesis, Characterization and Cu2+ Binding Studies of I-Histidine Ester of 8-Hydroxyquinoline. *InorganicaChimicaActa* 2014, 423, 72–78.
- 26. Dammak, T.; Fourati, N.; Abid, Y.; Boughzala, H.; Mlayah, A.; Minot, C. Structural, Vibrational and Ab Initio Studies of I-Histidine Oxalate. Spectrochim. Acta Part A: Mol. Biomol. Spectrosc. 2007, 66, 1097-1101
- 27. Sun, G. H.; Zhang, G. H.; Wang, X. Q.; Xu, D. Nucleation Kinetics, Micro-Crystallization and Etching Studies of I-Histidine Trifluoroacetate Crystal. J. Cryst. Grow. 2011, 316, 132-136.
- 28. De Sousa, G. P.; Freire, P. T. C.; Lima, Jr., J. A.; Mendes Filho, J.; Melo, F. E. A. High-Pressure Raman Spectra of I-Histidine Hydrochloride Monohydrate Crystal. Vib. Spectrosc. 2011, 57, 102-107.
- 29. Robert, R.; Justin Raj, C.; Krishnan, S.; Uthrakumar, R.; Dinakaran, S.; Jerome Das, S. Spectral, Optical and Mechanical Studies on I-Histidine Hydrochloride Monohydrate (LHC) Single Crystals Grown by

- Unidirectional Growth Technique. Physica B: Condens. Matter. 2010, 405, 3248-3252.
- 30. Thayanithi, V.; Praveen Kumar, P. Unidirectional Growth, Optical and Dielectrical Behavior of Nicotinium p-Toluenesulfonate Crystal for Optoelectronic Applications. Mater. Lett. 2021, 285, 129189.
- 31. Thejashwini, B. R.; Vijay, K.; Madhusudhana, R.; Sahoo, B. Crystal Growth and Effect of Defects on the Dielectric Properties of Ammonium Dihydrogen Phosphate (ADP) Single Crystals. J. Mater. Sci.: Mater. Electron. 2020, 31, 10548-10552.
- 32. RajKumar, R.; Praveen Kumar, P. Thermal, Mechanical, Optical and Dielectric Properties of Piperazinium Hydrogen Phosphite Monohydrate NLO Single Crystal. Appl. Phys. A 2018, 124, 382.
- 33. Albert, H. M.; Padmavathi, P.; Mahalakshmi, A.; Srinivas, G. V. S.; Chakravarthi, M. K.; Babu, M. R.; Kumar, M. N. Alosious Gonsago, C. Exploring the Spectroscopic, Photoluminescence, Thermal, Dielectric,

- and Electrical Conductivity Properties of 4-Aminopyridine Nitrate (4APN): A Semi-organic Material. J. Mater. Res. 2025 40, 452-462.
- 34. Hussam, B.; Nasr, H.; Najat, B.; Hayat, S.; Mohammed, N. B.; Farid, A.; Taj-dine, L.; Mohammed, B.; Mustapha, A. Dielectric Properties, AC Conductivity, and Electric Modulus Analysis of Bulk Ethylcarbazole-Terphenyl. Adv. Mater. Sci. Eng. 2020, 2020, 8.
- 35. Zhao, J.; Wang, F.; Huang, P.; Lu, T. J.; Xu, K. W. Depth Dependent Strain Rate Sensitivity and Inverse Indentation Size Effect of Hardness in body-centered Cubic Nanocrystalline Metals. Mater. Sci. Eng.: A 2014, *615*, 87-91.
- 36. Krishna mohan, M.; Ponnusamy, S.; Muthamizhchelvan, C. Spectral, Optical, Etching, Second Harmonic Generation (SHG) and Laser Damage Threshold Studies of Nonlinear Optical Crystals of I-Histidine Bromide. Appl. Surf. Sci. 2018, 449, 92-95.